nature chemical engineering

Supplementary information https://doi.org/10.1038/s44286-025-00249-z

Flow-driven data intensification to accelerate autonomous inorganic materials discovery

In the format provided by the authors and unedited

Table of Contents

1. Residence Time Distribution Experiments

The residence time distribution (RTD) of the designed microreactor was experimentally investigated to characterize the system's flow behavior and evaluate the extent of axial dispersion. RTD experiments were conducted using a step-input methodology where a solution of Sudan Blue II in 1-octadecene (ODE) and pure ODE were separately pumped into a T-mixer (IDEX, U-428) positioned at the inlet of the flow reactor module. The RTD experiments were performed at nominal residence times of 0.5 min and 9 min, covering the boundaries of the volumetric flow rate parameter space studied in this work. Additional verification experiments were conducted at intermediate residence times (1 min, 2 min, and 8 min) to ensure consistent behavior. For each RTD experiment, the system was first allowed to reach a steady state at an initial ratio of pure ODE to Sudan Blue II solution of 3:1, followed by a step change to a new ratio of 1:3 while maintaining a constant total volumetric flow rate. The downstream dispersion of the step change was monitored using *in-situ* UV-Vis absorption spectroscopy at 647 nm with the same setup described in the main text. All RTD experiments were conducted with the flow reactor maintained at 250 °C, matching typical reaction conditions studied in this work.

The experimental data was transformed into an *F*-curve by normalizing the detector response from 0 to 1 as a function of time. Subsequently, the *F*-curve was regressed against the dispersion model (***Equation 1***) described by Levenspiel using Levenberg-Marquardt Algorithm (curve_fit from Sci-Py package) to determine the Bodenstein number (*Bo*) and the average residence time (t_{avg}). The Bodenstein number serves as a metric for deviation of the flow behavior inside the flow reactor from ideal plug-flow behavior, where values above 100 indicate small deviations from plug flow. [1]

$$F(t^*) = \frac{1}{2}\left[\mathrm{erf}\left(\sqrt{\frac{Bo}{4}}\left(\frac{t}{t_{avg}} - 1\right)\right) + \mathrm{erf}\left(\sqrt{\frac{Bo}{4}}\right)\right]$$

(Supplementary Equation 1)

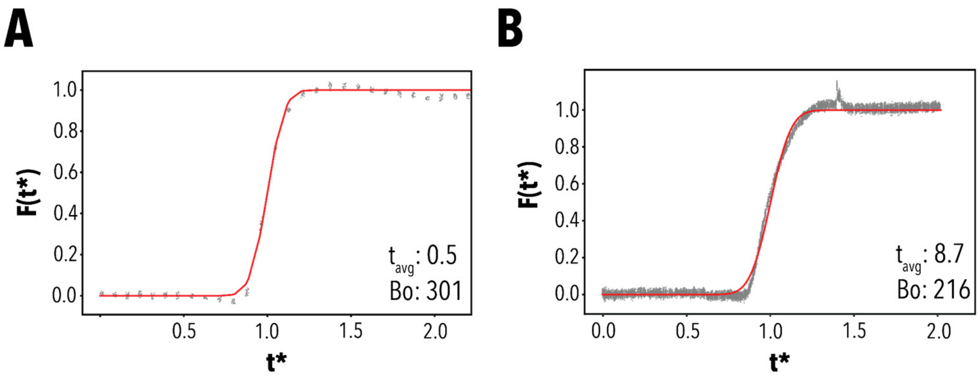

Supplementary Figure 1. Residence Time Distribution Experiments. *Normalized residence time distribution (F-curve) obtained from step-input experiments at a nominal residence time of (A) 0.5 min and (B) 9 min at 250 °C. Grey dots represent experimental UV absorbance data normalized between 0 and 1, while the red line shows the fitted dispersion model. The regressed parameters indicate an average residence time (t_{avg}) of 0.5 min and 8.7 min, respectively; and a Bo number of 301.8 and 216.5 for panels (A) and (B), respectively, confirming near plug-flow behavior for the entire range of the volumetric flow rates tested in this work. The dimensionless time (t*) represents the actual time divided by the average residence time ($t^* = t/t_{avg}$).*

The experimentally determined *Bo* numbers were 301.8 and 216.5 for residence times of 1 min and 9 min, respectively (**Supplementary Figure 1**). These *Bo* values exceed the threshold for plug-flow behavior, confirming that the flow reactor operates in a near-ideal plug-flow regime under the investigated experimental conditions. The regressed mean residence times (0.5 min and 8.7 min) showed excellent agreement with the expected nominal residence times (0.5 min and 9 min) calculated from the flow reactor volume and the set volumetric flow rates.

The narrow RTD and high *Bo* numbers obtained from the RTD experiments can be attributed to the geometry of the flow reactor, which promotes enhanced mixing conditions. The coil flow inverter (CFI) reactor design, used in this work, contains helical coil sections that induce secondary flows, known as *Dean* flow, arising from the centrifugal forces experienced by the fluid as it traverses the curved path. These secondary flows manifest as counter-rotating vortices perpendicular to the primary flow direction, significantly improving radial mixing. [2] Additionally, the incorporation of 90-degree bends between coil sections introduces chaotic advection, further enhancing the mixing efficiency. Reactor design parameters such as turns per coiled section (3–4 turns), as well as pitch distance (<4 mm) and curvature ratio ($C_r = D_C/D_i \sim 4$) between the diameter of the curvature ($D_C \sim 3.175$ mm) and the diameter of the tube ($D_i = 0.762$ mm), were chosen based on previous literature shown to improve RTD. [2-5] The CFI microreactor used in this study is shown in **Supplementary Figure 2**.

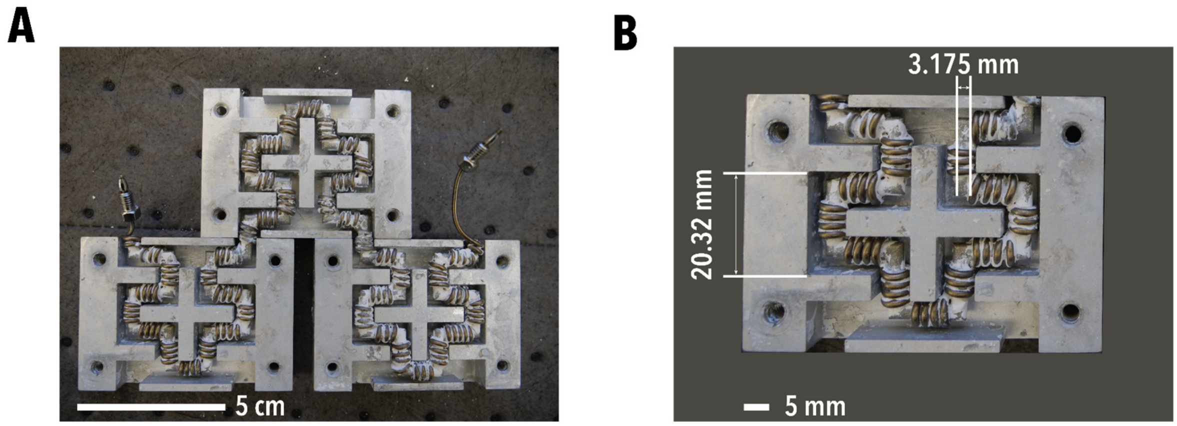

Supplementary Figure 2. **Design and Characterization of the Flow Reactor Module.** *(A) A photograph of the machined aluminum reactor block housing the CFI microreactor module. (B) Single CFI microreactor module with key design parameters highlighted.*

2. Initial Parameter Space Sampling

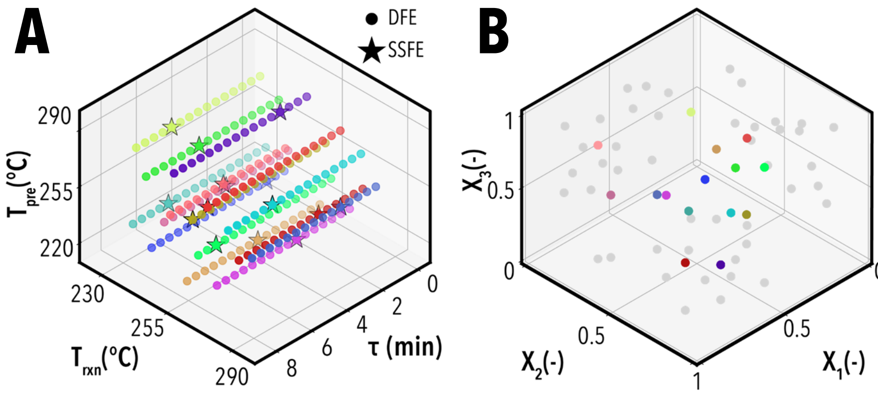

Supplementary Figure 3. **Latin Hypercube Sampling (LHS) Parameter Space Sampling.** *(A) Comparison between Dynamic Flow Experiments (DFE) and Steady-State Flow Experiments (SSFE) represented by circles and stars, respectively, with an initialization budget of 15 experiments. Color-coded by distinct* X_1, X_2, *and* X_3, *values, that map to hue, saturation, and value respectively in the HSV color space. (B)* X_1, X_2, *and* X_3 *LHS samples explored in initialization data. Light gray dots represent the projection of each pair of X dimensions.*

3. Shapley Additive Explanation Analysis

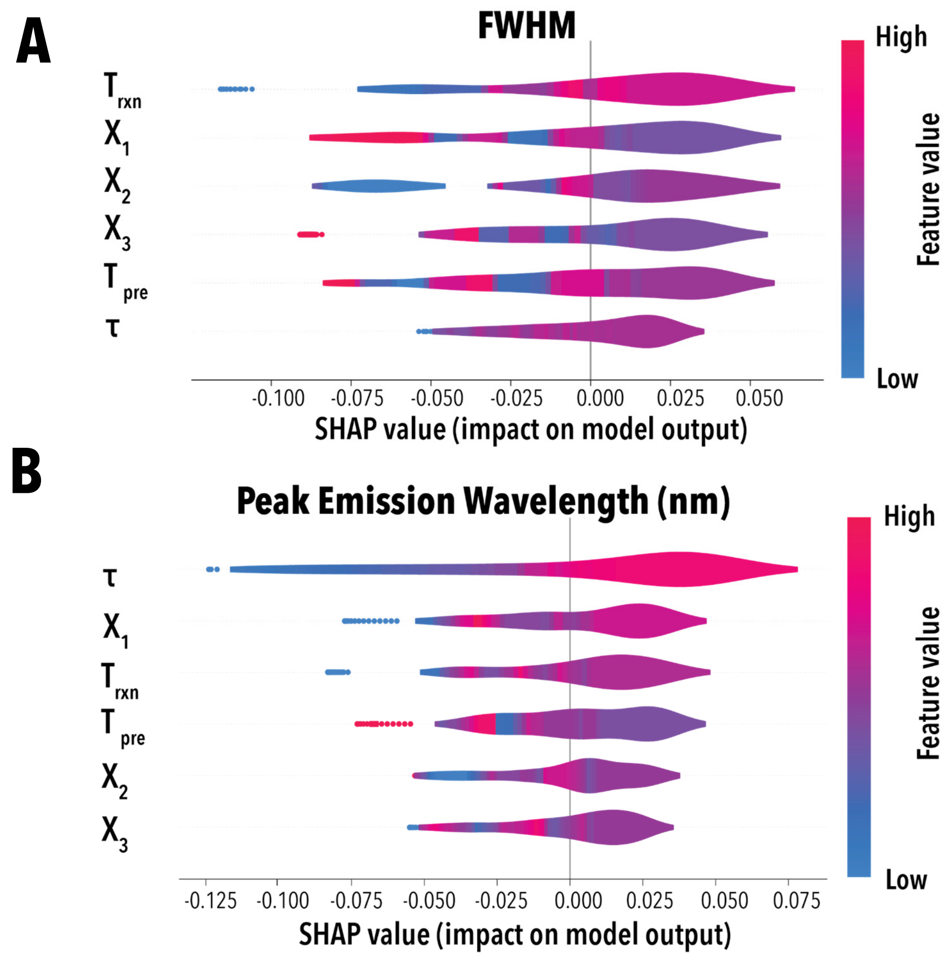

Supplementary Figure 4. **Shapley Additive Explanation (SHAP) Analysis of the In-Flow CdSe QD Synthesis.** *Impact of process variables, including the reactor temperature (T_{rxn}), the preheater temperature (T_{pre}), cadmium dilution (X_1), selenium dilution (X_2) and cadmium to selenium volumetric flow rate ratio (X_3) on the (A) λ_{em} and (B) FWHM of the in-flow synthesized CdSe QDs. Positive SHAP values indicate peak narrowing and negative values indicate peak broadening. The color gradient represents the magnitude of each feature value (blue = low, red = high) and the width of each violin plot indicates the density of data points at that SHAP value.*

4. DFE vs. SSFE Mapping

The mapping of t_m and τ follows the derivation of Moore and Jensen.[6] **Supplementary Equation 2** reproduces their correction for τ under a linear ramp, accounting for the dead volume in the fluidic path.

$$\tau = e^{-\frac{V_d}{V_r}\alpha} t_m - \left(1 - e^{-\frac{V_d}{V_r}\alpha}\right)\frac{\tau_0}{\alpha} - \tau_0\left(\frac{1}{\alpha}\ln\left(\frac{\tau_0 + \alpha\left(e^{-\frac{V_d}{V_r}\alpha} t_m - \left(1 - e^{-\frac{V_d}{V_r}\alpha}\right)\frac{\tau_0}{\alpha}\right)}{\tau_0}\right) - 1\right)$$

(Supplementary Equation 2)

This correction is applied until the time that the last fluidic element that experiences part of the steady-state (before the dynamic ramp) exits the microreactor (t^*). Following the approach of Moore and Jensen,[6] we apply this correction until **Supplementary Equation 2** intercepts **Equation 2**. This value has been calculated by Florit *et al.*, [7] and is given by **Supplementary Equation 3**.

(Supplementary Equation 3)

$$t^* = \frac{e^{\alpha\tau_0} - 1}{\alpha}$$

The DFE results, shown in **Figure 2** of the main text, were conducted over a duration of approximately 20 min. Applying **Equation 2** (main text) with t_m = 20 min results in $\tau_{max} \approx 8.5$ min, enabling continuous sampling across reaction (residence) times ranging from 1 min to 8.5 min. For comparative analysis, a measurement at t_m = 10 min would correspond to a hypothetical steady-state flow experiment (SSFE) with a $\tau \approx 4.65$ min. Allowing for system equilibration (4τ), the complete SSFE parameter-synthesis property mapping requires approximately 18.6 min.

The total material consumption is quantified by integrating the volumetric flow rate over the experimental duration. For SSFE, integration from t = 0 to t = 18.6 min yields 4.5 mL. Similarly, for DFE, integration of the flow rate (calculated as V_r/**Equation 1** from main text) from t = 0 to t_m = 20 min results in 4.758 mL.

The difference in material consumption and processing time between methodologies is ≤ 7% for this scenario. Notably, the DFE methodology enables continuous synthesis-property mapping across the residence time domain (1 min-8.5 min) with temporal resolution of <1 s, offering significantly enhanced sampling density compared to discrete SSFE measurements.

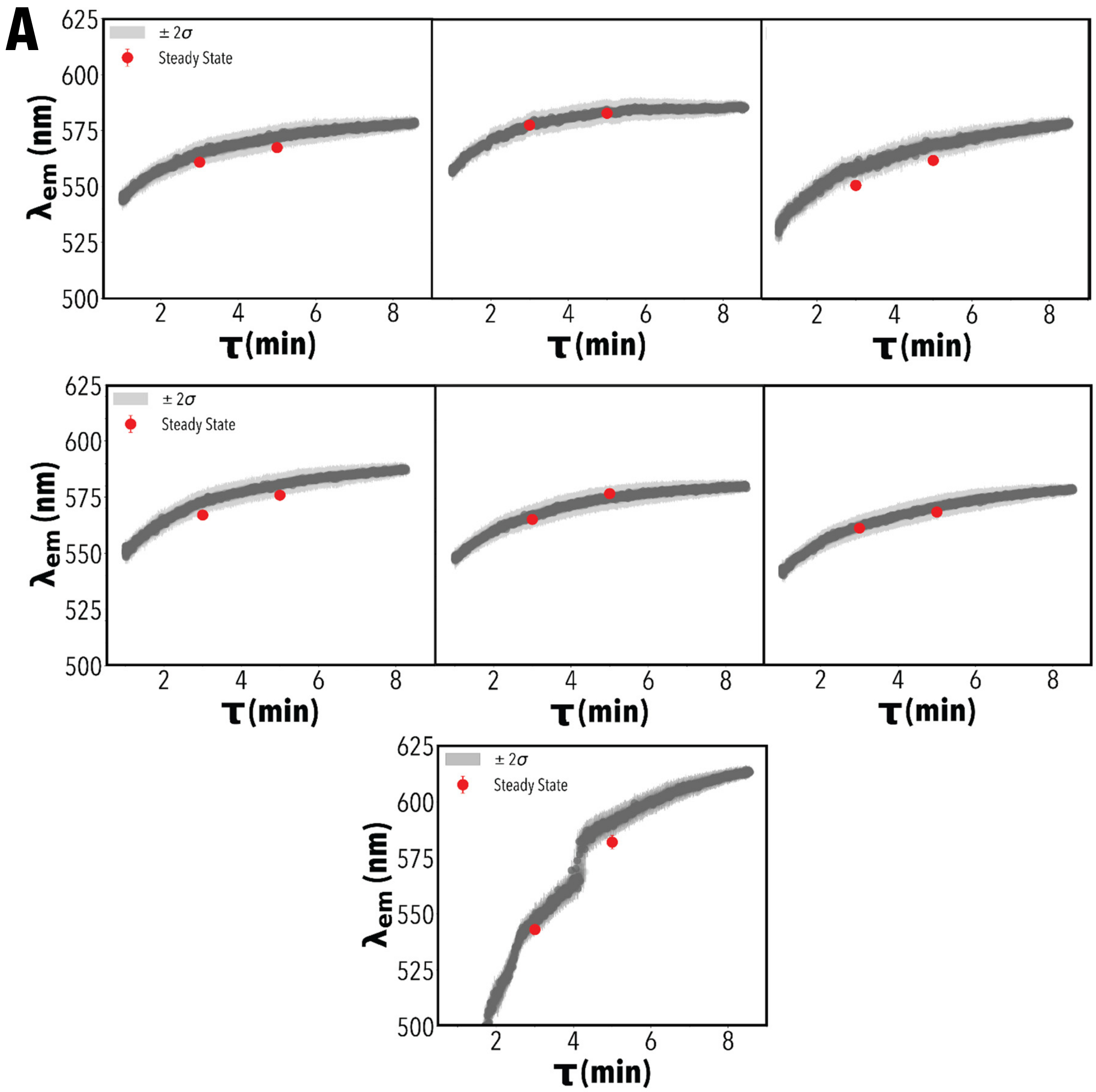

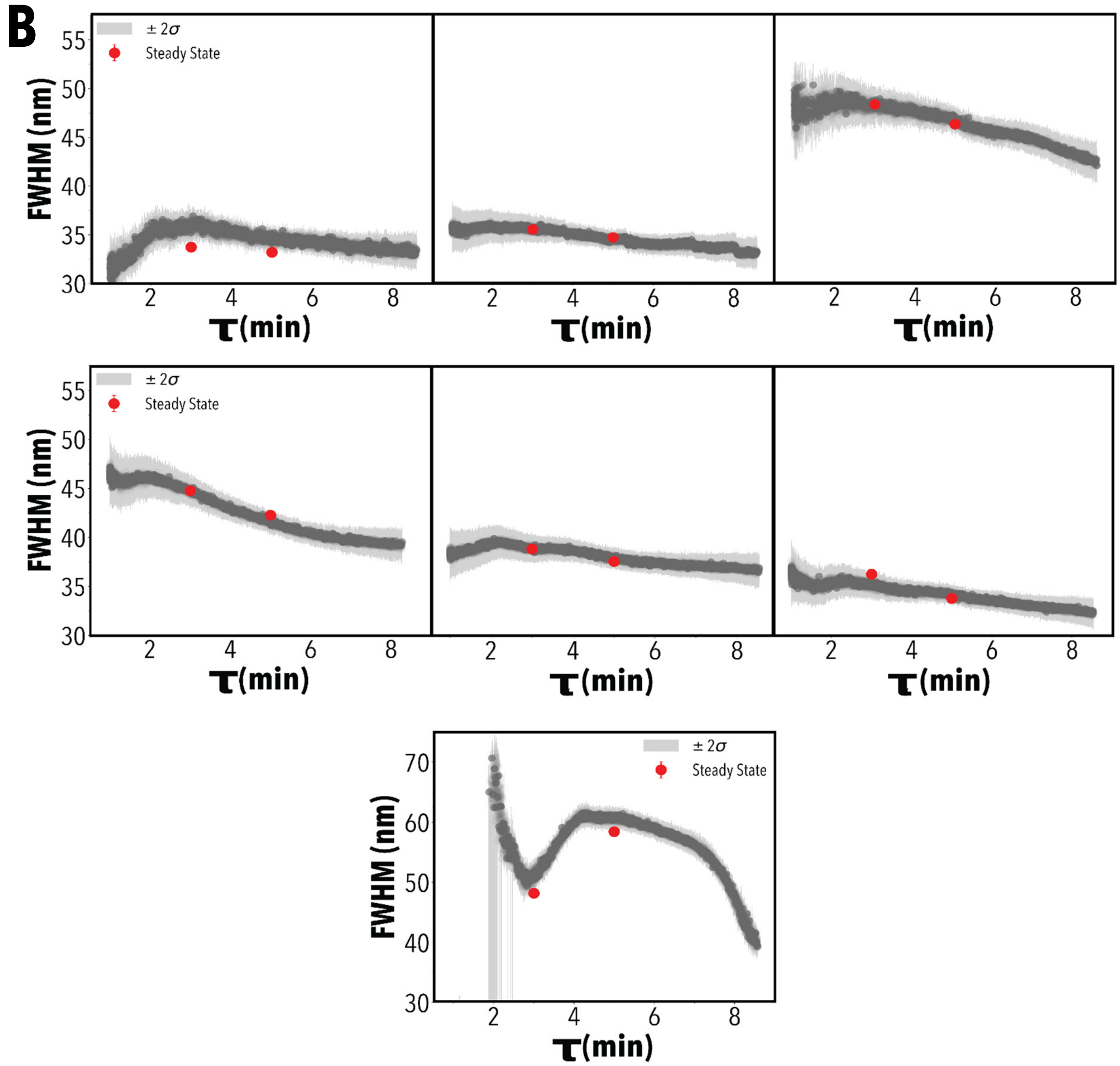

Supplementary Figure 5. **Transient-to-Steady-State Mapping Validation.** *Comparison between dynamic flow ramp data (gray points) and the mean value over 15 s of steady-state measurements (red points) for (A) λ_{em} and (B) FWHM across seven randomly selected LHS initialization samples. Steady-state data was collected at 3 min and 5 min residence times. The light gray area represents the average experimental standard deviation of a dynamic experiment performed multiple times, accounting for experiment-to-experiment and day-to-day variability. Error bars at steady-state represent standard deviation of 15 s after the system has reached steady-state.*

In order to assess the uncertainty of the DFE to SSFE mapping, we quantified uncertainties for each experimental component. First, non-idealities like precursor degradation that could occur over time were characterized by repeating a steady-state control experiment throughout the autonomous QD synthesis campaign, **Supplementary Table 1.**

Supplementary Table 1. *Control SSFE experiments during autonomous QD synthesis*

Replicate #	Tau (min)	Tpre (°C)	Trxn (°C)	Cd (µL/min)	Se (µL/min)	CdODE (µL/min)	SeODE (µL/min)	λem (nm)	FWHM (nm)
1	1.00	227.00	284.00	245.77	79.39	569.16	218.66	544.63	38.15
2	1.00	227.00	284.00	245.77	79.39	569.16	218.66	544.45	43.43
3	1.00	227.00	284.00	245.77	79.39	569.16	218.66	542.26	43.27
4	1.00	227.00	284.00	245.77	79.39	569.16	218.66	543.17	41.16
5	1.00	227.00	284.00	245.77	79.39	569.16	218.66	542.97	39.24
6	1.00	227.00	284.00	245.77	79.39	569.16	218.66	546.63	39.27
7	1.00	227.00	284.00	245.77	79.39	569.16	218.66	543.12	41.20
8	1.00	227.00	284.00	245.77	79.39	569.16	218.66	543.71	38.85
9	1.00	227.00	284.00	245.77	79.39	569.16	218.66	544.29	42.47
AVG.	**1.00**	**227.00**	**284.00**	**245.77**	**79.39**	**569.16**	**218.66**	**543.91**	**40.78**
STD.DEV.								**1.21**	**1.88**

Analysis of the control SSFE experiments revealed an average standard deviation of ~1.2 nm and ~1.9 nm for λ_{em} and *FWHM*, respectively, for replicates of the same SSFE. Next, a baseline DFE was repeated over different days to investigate potential fluid delivery (*i.e.,* syringe pumps) non-uniformities. The results of this set of DFE experiments are shown as the gray area surrounding the mean trajectory in **Figure 3a** and **3b** of the main text. After applying the DFE to SSFE mapping, the average standard deviation observed over any given 1.15 s interval in the baseline DFE is ~1.9 nm and 0.6 nm for λ_{em} and *FWHM*, respectively

Lastly, to quantify the prediction error originating from using a DFE to predict SSFE properties, we analyzed the 21 paired experiments directly comparing transient data from the DFE (mapped to SSFE using **Equations 8** and **2** (from main text)) *vs*. independent SSFEs at identical τ. The results of these experiments are presented in **Figures 2** and **Supplementary Figure 5** and summarized in **Supplementary Table 2**. The RMSE of the DFE-measured steady-state property *vs*. a SSFE for the same QD synthesis condition is 4.1 nm. From an inorganic nanomaterial synthesis perspective, an RMSE of ~4 nm to unlock >10× improvement on material consumption and processing time is considered as one of the strongest attributes of DFE. The SSFE prediction from DFE *vs.* ground-truth SSFE error represents a normalized RMSE of less than <5% across the full range of λ_{em} explored.

To highlight the efficiency gains enabled by DFEs in experimental data generation of inorganic materials, the entire dataset obtained from the DFEs (with a 30 s interval), used to initialize the surrogate ML model of the closed-loop experimentation campaigns, are presented in **Supplementary Table 3**. It should be noted that a higher sampling rate (*i.e.*, a shorter interval) could also be utilized (~13,700 experimental data points were generated with a sub-second resolution per DFE), but at a higher computational cost for training the surrogate ML model.[8]

Utilizing the data presented in **Supplementary Table 3**, we compared the total amount of precursor consumption and operational time it would have taken if each data were to be obtained under SSFE. For this comparison, we assumed steady state is reached at the end of $4\times\tau$ and the characterization time is negligible. **Supplementary Table 4** summarizes the results of this comparison and demonstrates that DFE is >10× more material- and time-efficient than SSFE at replicating a similar experimental dataset.

Supplementary Table 2. *DFE-measured steady-state QD properties vs. SSFE for the mapped QD synthesis condition.*

Experiment	DFE λem (nm)	SSFE λem (nm)	Tau (min)	Square Error
1	542.5	544.9	1	5.5
2	554.8	556.5	2	2.6
3	563.4	562.5	3	0.9
4	570.3	571.9	4	2.4
5	576.4	572.4	5	15.7
6	579.7	577.6	6	4.2
7	582.5	580.4	7	4.4
8	564.9	560.9	3	16.5
9	572.2	567.3	5	24.1
10	572.8	567.0	3	33.7
11	580.8	575.9	5	24.2
12	547.1	543.0	3	16.4
13	590.8	582.0	5	76.7
14	562.1	561.5	3	0.4
15	571.1	568.8	5	5.2
16	558.7	551.1	3	58.3
17	569.3	562.1	5	51.0
18	578.1	577.7	3	0.2
19	583.9	583.1	5	0.6
20	567.0	565.6	3	2.1
21	575.3	577.1	5	3.3
Square Root Average				4.1

Supplementary Table 3. *Initialization dataset from DFE-LHS.*

Tau (min)	Tpre (°C)	Trxn (°C)	Cd (µL/min)	Se (µL/min)	CdODE (µL/min)	SeODE (µL/min)	λem (nm)	FWHM (nm)
1.00	259.00	226.00	122.18	199.10	413.07	378.65	515.66	39.34
1.50	259.00	226.00	81.46	132.73	275.38	252.43	527.19	42.26
2.00	259.00	226.00	61.09	99.55	206.54	189.33	536.11	45.43
2.50	259.00	226.00	48.87	79.64	165.23	151.46	541.65	46.88
3.00	259.00	226.00	40.73	66.37	137.69	126.22	545.43	47.92
3.50	259.00	226.00	34.91	56.88	118.02	108.19	549.66	48.32
4.00	259.00	226.00	30.55	49.77	103.27	94.66	551.97	48.82
4.50	259.00	226.00	27.15	44.24	91.79	84.14	554.92	48.80
5.00	259.00	226.00	24.44	39.82	82.61	75.73	557.16	48.78
5.50	259.00	226.00	22.22	36.20	75.10	68.85	558.08	48.77
6.00	259.00	226.00	20.36	33.18	68.85	63.11	561.56	48.72
6.50	259.00	226.00	18.80	30.63	63.55	58.25	559.90	49.05
7.00	259.00	226.00	17.45	28.44	59.01	54.09	563.16	48.45
7.50	259.00	226.00	16.29	26.55	55.08	50.49	566.71	48.19
8.00	259.00	226.00	15.27	24.89	51.63	47.33	567.87	47.93
8.50	259.00	226.00	14.37	23.42	48.60	44.55	568.57	47.50
1.00	275.00	234.00	425.03	240.15	202.54	245.28	538.24	46.61
1.50	275.00	234.00	283.35	160.10	135.03	163.52	549.91	45.36

2.00	275.00	234.00	212.52	120.07	101.27	122.64	557.27	46.08
2.50	275.00	234.00	170.01	96.06	81.02	98.11	562.36	46.19
3.00	275.00	234.00	141.68	80.05	67.51	81.76	567.18	45.89
3.50	275.00	234.00	121.44	68.61	57.87	70.08	570.30	45.43
4.00	275.00	234.00	106.26	60.04	50.64	61.32	572.62	44.83
4.50	275.00	234.00	94.45	53.37	45.01	54.51	574.83	44.25
5.00	275.00	234.00	85.01	48.03	40.51	49.06	576.98	43.45
5.50	275.00	234.00	77.28	43.66	36.83	44.60	578.89	43.02
6.00	275.00	234.00	70.84	40.02	33.76	40.88	580.15	42.83
6.50	275.00	234.00	65.39	36.95	31.16	37.74	580.89	42.43
7.00	275.00	234.00	60.72	34.31	28.93	35.04	582.42	41.97
7.50	275.00	234.00	56.67	32.02	27.01	32.70	583.47	41.67
8.00	275.00	234.00	53.13	30.02	25.32	30.66	584.49	41.33
8.50	275.00	234.00	50.00	28.25	23.83	28.86	585.57	40.97
1.00	240.00	234.00	442.25	214.89	326.51	129.35	513.99	45.54
1.50	240.00	234.00	294.83	143.26	217.67	86.24	525.72	52.27
2.00	240.00	234.00	221.12	107.45	163.25	64.68	534.44	56.73
2.50	240.00	234.00	176.90	85.96	130.60	51.74	542.70	57.12
3.00	240.00	234.00	147.42	71.63	108.84	43.12	547.37	57.35
3.50	240.00	234.00	126.36	61.40	93.29	36.96	560.62	56.03
4.00	240.00	234.00	110.56	53.72	81.63	32.34	564.33	54.72

4.50	240.00	234.00	98.28	47.75	72.56	28.75	566.78	53.93
5.00	240.00	234.00	88.45	42.98	65.30	25.87	569.94	53.24
5.50	240.00	234.00	80.41	39.07	59.36	23.52	572.52	52.52
6.00	240.00	234.00	73.71	35.82	54.42	21.56	574.21	51.80
6.50	240.00	234.00	68.04	33.06	50.23	19.90	575.85	51.25
7.00	240.00	234.00	63.18	30.70	46.64	18.48	577.81	50.26
7.50	240.00	234.00	58.97	28.65	43.53	17.25	579.49	49.02
8.00	240.00	234.00	55.28	26.86	40.81	16.17	581.07	48.06
8.50	240.00	234.00	52.03	25.28	38.41	15.22	582.23	47.33
1.00	230.00	242.00	140.89	343.08	158.55	470.47	531.94	48.07
1.50	230.00	242.00	93.93	228.72	105.70	313.65	541.98	47.97
2.00	230.00	242.00	70.45	171.54	79.28	235.23	549.81	47.87
2.50	230.00	242.00	56.36	137.23	63.42	188.19	555.85	48.71
3.00	230.00	242.00	46.96	114.36	52.85	156.82	560.22	48.27
3.50	230.00	242.00	40.26	98.02	45.30	134.42	560.46	47.87
4.00	230.00	242.00	35.22	85.77	39.64	117.62	564.05	47.56
4.50	230.00	242.00	31.31	76.24	35.23	104.55	567.18	47.22
5.00	230.00	242.00	28.18	68.62	31.71	94.09	569.31	46.59
5.50	230.00	242.00	25.62	62.38	28.83	85.54	570.24	45.73
6.00	230.00	242.00	23.48	57.18	26.43	78.41	572.07	45.40
6.50	230.00	242.00	21.68	52.78	24.39	72.38	573.48	45.04

7.00	230.00	242.00	20.13	49.01	22.65	67.21	574.39	44.51
7.50	230.00	242.00	18.79	45.74	21.14	62.73	576.42	43.83
8.00	230.00	242.00	17.61	42.89	19.82	58.81	577.64	43.03
8.50	230.00	242.00	16.58	40.36	18.65	55.35	578.53	42.44
1.00	265.00	246.00	363.46	188.53	518.12	42.89	521.44	48.19
1.50	265.00	246.00	242.31	125.69	345.41	28.59	534.69	54.77
2.00	265.00	246.00	181.73	94.27	259.06	21.44	539.59	56.77
2.50	265.00	246.00	145.38	75.41	207.25	17.16	546.55	57.94
3.00	265.00	246.00	121.15	62.84	172.71	14.30	554.78	58.35
3.50	265.00	246.00	103.85	53.87	148.03	12.25	562.54	58.44
4.00	265.00	246.00	90.86	47.13	129.53	10.72	568.29	58.38
4.50	265.00	246.00	80.77	41.90	115.14	9.53	572.32	58.06
5.00	265.00	246.00	72.69	37.71	103.62	8.58	575.61	57.79
5.50	265.00	246.00	66.08	34.28	94.20	7.80	578.74	57.34
6.00	265.00	246.00	60.58	31.42	86.35	7.15	581.97	56.65
6.50	265.00	246.00	55.92	29.01	79.71	6.60	584.07	55.34
7.00	265.00	246.00	51.92	26.93	74.02	6.13	584.67	54.58
7.50	265.00	246.00	48.46	25.14	69.08	5.72	586.45	54.29
8.00	265.00	246.00	45.43	23.57	64.76	5.36	587.47	53.34
8.50	265.00	246.00	42.76	22.18	60.96	5.05	588.41	51.69
1.00	242.00	248.00	352.87	144.64	124.23	491.26	516.41	45.28

1.50	242.00	248.00	235.24	96.43	82.82	327.51	528.96	50.66
2.00	242.00	248.00	176.43	72.32	62.12	245.63	539.52	54.12
2.50	242.00	248.00	141.15	57.86	49.69	196.50	544.63	56.32
3.00	242.00	248.00	117.62	48.21	41.41	163.75	548.73	57.49
3.50	242.00	248.00	100.82	41.33	35.50	140.36	550.91	58.08
4.00	242.00	248.00	88.22	36.16	31.06	122.82	554.93	58.68
4.50	242.00	248.00	78.41	32.14	27.61	109.17	557.96	59.75
5.00	242.00	248.00	70.57	28.93	24.85	98.25	562.37	60.69
5.50	242.00	248.00	64.16	26.30	22.59	89.32	578.35	60.27
6.00	242.00	248.00	58.81	24.11	20.71	81.88	580.50	59.56
6.50	242.00	248.00	54.29	22.25	19.11	75.58	582.60	59.17
7.00	242.00	248.00	50.41	20.66	17.75	70.18	584.20	58.68
7.50	242.00	248.00	47.05	19.29	16.56	65.50	585.43	58.46
8.00	242.00	248.00	44.11	18.08	15.53	61.41	586.65	57.75
1.00	282.00	251.00	287.74	540.49	76.26	208.51	550.80	46.50
1.50	282.00	251.00	191.83	360.32	50.84	139.01	558.27	45.93
2.00	282.00	251.00	143.87	270.24	38.13	104.26	563.96	46.08
2.50	282.00	251.00	115.10	216.19	30.50	83.40	568.45	45.54
3.00	282.00	251.00	95.91	180.16	25.42	69.50	572.77	44.75
3.50	282.00	251.00	82.21	154.42	21.79	59.57	575.46	43.84
4.00	282.00	251.00	71.94	135.12	19.06	52.13	576.85	43.05

4.50	282.00	251.00	63.94	120.11	16.95	46.34	579.17	42.36
5.00	282.00	251.00	57.55	108.10	15.25	41.70	580.79	41.31
5.50	282.00	251.00	52.32	98.27	13.87	37.91	582.32	40.82
6.00	282.00	251.00	47.96	90.08	12.71	34.75	583.90	40.42
6.50	282.00	251.00	44.27	83.15	11.73	32.08	584.50	40.08
7.00	282.00	251.00	41.11	77.21	10.89	29.79	585.31	39.70
7.50	282.00	251.00	38.37	72.06	10.17	27.80	585.69	39.47
8.00	282.00	251.00	35.97	67.56	9.53	26.06	587.19	39.35
1.00	289.00	257.00	234.11	224.87	183.81	470.21	532.61	49.33
1.50	289.00	257.00	156.07	149.91	122.54	313.47	543.22	48.98
2.00	289.00	257.00	117.06	112.43	91.91	235.10	548.71	49.73
2.50	289.00	257.00	93.64	89.95	73.52	188.08	554.08	50.28
3.00	289.00	257.00	78.04	74.96	61.27	156.74	557.80	50.60
3.50	289.00	257.00	66.89	64.25	52.52	134.35	561.31	50.82
4.00	289.00	257.00	58.53	56.22	45.95	117.55	565.45	50.25
4.50	289.00	257.00	52.02	49.97	40.85	104.49	565.81	50.57
5.00	289.00	257.00	46.82	44.97	36.76	94.04	568.81	49.75
5.50	289.00	257.00	42.57	40.89	33.42	85.49	571.20	48.95
6.00	289.00	257.00	39.02	37.48	30.64	78.37	573.01	48.02
6.50	289.00	257.00	36.02	34.60	28.28	72.34	575.13	47.33
7.00	289.00	257.00	33.44	32.12	26.26	67.17	576.78	46.01

7.50	289.00	257.00	31.21	29.98	24.51	62.69	577.88	45.04
8.00	289.00	257.00	29.26	28.11	22.98	58.78	579.09	44.46
2.00	250.00	261.00	341.15	24.01	93.28	98.05	514.31	57.14
2.50	250.00	261.00	272.92	19.21	74.63	78.44	534.48	54.92
3.00	250.00	261.00	227.44	16.01	62.19	65.37	548.36	51.11
3.50	250.00	261.00	194.95	13.72	53.30	56.03	555.72	55.84
4.00	250.00	261.00	170.58	12.01	46.64	49.03	564.74	60.07
4.50	250.00	261.00	151.62	10.67	41.46	43.58	585.89	60.85
5.00	250.00	261.00	136.46	9.60	37.31	39.22	591.22	60.84
5.50	250.00	261.00	124.06	8.73	33.92	35.66	595.92	60.09
6.00	250.00	261.00	113.72	8.00	31.09	32.68	600.43	59.04
6.50	250.00	261.00	104.97	7.39	28.70	30.17	604.20	57.66
7.00	250.00	261.00	97.47	6.86	26.65	28.01	606.87	56.26
7.50	250.00	261.00	90.97	6.40	24.88	26.15	608.97	53.22
8.00	250.00	261.00	85.29	6.00	23.32	24.51	611.61	47.44
8.50	250.00	261.00	80.27	5.65	21.95	23.07	613.16	41.16
1.00	262.00	266.00	59.97	499.48	164.90	388.64	544.81	31.59
1.50	262.00	266.00	39.98	332.99	109.94	259.10	552.26	33.01
2.00	262.00	266.00	29.99	249.74	82.45	194.32	557.40	35.26
2.50	262.00	266.00	23.99	199.79	65.96	155.46	560.95	35.53
3.00	262.00	266.00	19.99	166.49	54.97	129.55	565.07	35.99

3.50	262.00	266.00	17.13	142.71	47.12	111.04	567.26	35.67
4.00	262.00	266.00	14.99	124.87	41.23	97.16	568.49	35.32
4.50	262.00	266.00	13.33	111.00	36.65	86.37	569.99	34.71
5.00	262.00	266.00	11.99	99.90	32.98	77.73	572.34	34.48
5.50	262.00	266.00	10.90	90.81	29.98	70.66	573.57	34.11
6.00	262.00	266.00	10.00	83.25	27.48	64.77	574.99	34.13
6.50	262.00	266.00	9.23	76.84	25.37	59.79	575.34	33.86
7.00	262.00	266.00	8.57	71.35	23.56	55.52	575.69	33.82
7.50	262.00	266.00	8.00	66.60	21.99	51.82	577.42	33.65
8.00	262.00	266.00	7.50	62.44	20.61	48.58	577.46	33.49
8.50	262.00	266.00	7.06	58.76	19.40	45.72	578.51	33.17
1.00	252.00	288.00	168.48	653.42	98.71	192.39	557.54	35.66
1.50	252.00	288.00	112.32	435.62	65.81	128.26	565.37	35.57
2.00	252.00	288.00	84.24	326.71	49.35	96.20	571.74	35.75
2.50	252.00	288.00	67.39	261.37	39.48	76.96	574.49	35.59
3.00	252.00	288.00	56.16	217.81	32.90	64.13	578.19	35.57
3.50	252.00	288.00	48.14	186.69	28.20	54.97	579.76	35.31
4.00	252.00	288.00	42.12	163.36	24.68	48.10	581.13	34.97
4.50	252.00	288.00	37.44	145.21	21.94	42.75	582.10	34.84
5.00	252.00	288.00	33.70	130.68	19.74	38.48	583.60	34.56
5.50	252.00	288.00	30.63	118.80	17.95	34.98	584.69	34.04

6.00	252.00	288.00	28.08	108.90	16.45	32.07	584.28	34.10
6.50	252.00	288.00	25.92	100.53	15.19	29.60	585.01	34.00
7.00	252.00	288.00	24.07	93.35	14.10	27.48	584.95	33.96
7.50	252.00	288.00	22.46	87.12	13.16	25.65	585.37	33.66
8.00	252.00	288.00	21.06	81.68	12.34	24.05	585.18	33.76
8.50	252.00	288.00	19.82	76.87	11.61	22.63	585.72	33.12
1.00	270.00	279.00	113.10	208.60	554.27	237.03	542.27	36.39
1.50	270.00	279.00	75.40	139.07	369.52	158.02	548.90	35.17
2.00	270.00	279.00	56.55	104.30	277.14	118.51	554.70	35.46
2.50	270.00	279.00	45.24	83.44	221.71	94.81	559.39	35.58
3.00	270.00	279.00	37.70	69.53	184.76	79.01	562.28	35.20
3.50	270.00	279.00	32.31	59.60	158.36	67.72	565.21	34.62
4.00	270.00	279.00	28.27	52.15	138.57	59.26	567.57	34.51
4.50	270.00	279.00	25.13	46.36	123.17	52.67	569.51	34.46
5.00	270.00	279.00	22.62	41.72	110.85	47.41	570.80	34.34
5.50	270.00	279.00	20.56	37.93	100.78	43.10	572.90	33.99
6.00	270.00	279.00	18.85	34.77	92.38	39.50	574.20	33.66
6.50	270.00	279.00	17.40	32.09	85.27	36.47	575.29	33.26
7.00	270.00	279.00	16.16	29.80	79.18	33.86	576.65	33.08
7.50	270.00	279.00	15.08	27.81	73.90	31.60	577.47	32.94
8.00	270.00	279.00	14.14	26.08	69.28	29.63	578.09	32.74

8.50	270.00	279.00	13.31	24.54	65.21	27.89	578.84	32.36
1.00	281.00	272.00	233.82	427.88	252.98	198.32	548.30	38.42
1.50	281.00	272.00	155.88	285.25	168.65	132.21	555.39	38.82
2.00	281.00	272.00	116.91	213.94	126.49	99.16	560.84	39.54
2.50	281.00	272.00	93.53	171.15	101.19	79.33	564.02	39.36
3.00	281.00	272.00	77.94	142.63	84.33	66.11	567.49	39.03
3.50	281.00	272.00	66.81	122.25	72.28	56.66	569.44	38.98
4.00	281.00	272.00	58.46	106.97	63.25	49.58	572.64	38.82
4.50	281.00	272.00	51.96	95.08	56.22	44.07	573.55	38.38
5.00	281.00	272.00	46.76	85.58	50.60	39.66	575.34	38.07
5.50	281.00	272.00	42.51	77.80	46.00	36.06	576.36	37.58
6.00	281.00	272.00	38.97	71.31	42.16	33.05	577.22	37.53
6.50	281.00	272.00	35.97	65.83	38.92	30.51	577.95	37.27
7.00	281.00	272.00	33.40	61.13	36.14	28.33	578.69	37.27
7.50	281.00	272.00	31.18	57.05	33.73	26.44	579.05	37.06
8.00	281.00	272.00	29.23	53.48	31.62	24.79	579.95	36.95
8.50	281.00	272.00	27.51	50.34	29.76	23.33	580.84	36.67
1.00	227.00	284.00	245.77	79.40	569.17	218.66	542.09	39.53
1.50	227.00	284.00	163.85	52.93	379.45	145.77	550.01	38.93
2.00	227.00	284.00	122.89	39.70	284.58	109.33	554.37	39.25
2.50	227.00	284.00	98.31	31.76	227.67	87.46	559.00	40.43

3.00	227.00	284.00	81.92	26.47	189.72	72.89	563.33	41.06
3.50	227.00	284.00	70.22	22.69	162.62	62.47	566.78	41.48
4.00	227.00	284.00	61.44	19.85	142.29	54.67	570.93	41.48
4.50	227.00	284.00	54.62	17.64	126.48	48.59	573.33	41.61
5.00	227.00	284.00	49.15	15.88	113.83	43.73	576.82	41.34
5.50	227.00	284.00	44.69	14.44	103.49	39.76	578.18	40.90
6.00	227.00	284.00	40.96	13.23	94.86	36.44	579.74	40.86
6.50	227.00	284.00	37.81	12.22	87.56	33.64	580.95	40.76
7.00	227.00	284.00	35.11	11.34	81.31	31.24	582.93	40.41
7.50	227.00	284.00	32.77	10.59	75.89	29.15	583.07	40.39
8.00	227.00	284.00	30.72	9.92	71.15	27.33	584.28	40.23
1.00	237.00	276.00	266.49	250.81	435.13	160.57	545.93	39.11
1.50	237.00	276.00	177.66	167.21	290.09	107.04	552.71	39.06
2.00	237.00	276.00	133.24	125.41	217.57	80.28	558.57	39.55
2.50	237.00	276.00	106.60	100.33	174.05	64.23	562.42	39.34
3.00	237.00	276.00	88.83	83.60	145.04	53.52	566.31	39.16
3.50	237.00	276.00	76.14	71.66	124.32	45.88	569.55	39.00
4.00	237.00	276.00	66.62	62.70	108.78	40.14	571.83	38.81
4.50	237.00	276.00	59.22	55.74	96.70	35.68	573.96	38.71
5.00	237.00	276.00	53.30	50.16	87.03	32.11	575.85	38.48
5.50	237.00	276.00	48.45	45.60	79.11	29.19	577.46	38.38

6.00	237.00	276.00	44.41	41.80	72.52	26.76	578.73	38.04
6.50	237.00	276.00	41.00	38.59	66.94	24.70	579.22	37.74
7.00	237.00	276.00	38.07	35.83	62.16	22.94	579.87	37.38
7.50	237.00	276.00	35.53	33.44	58.02	21.41	580.97	37.13
8.00	237.00	276.00	33.31	31.35	54.39	20.07	581.23	36.97
8.50	237.00	276.00	31.35	29.51	51.19	18.89	581.89	36.81

Supplementary Table 4. *Time and material consumption of DFE vs. SSFE.*

Ramp	SS Time (min)	DFE Time (min)	SS Volume (µL)	DFE Volume (µL)
1	304	24	71232	4457
2	304	24	71232	4457
3	304	24	71232	4457
4	304	24	71232	4457
5	304	24	71232	4457
6	270	24	66780	4457
7	270	24	66780	4457
8	270	24	66780	4457
9	294	24	66780	4457
10	304	24	71232	4457
11	304	24	71232	4457
12	304	24	71232	4457
13	304	24	71232	4457
14	270	24	66780	4457
15	304	24	71232	4457
SUM	**4414**	**360**	**1046220**	**66851**
× Factor		**12.3**		**15.6**

5. Generalizability of the DFE Strategy Beyond CdSe

To demonstrate broader applicability of the developed DFE strategy beyond CdSe QDs, we performed a similar DFE *vs.* SSFE mapping presented in **Supplementary Figure 5**, for a different class of inorganic material, indium phosphide (InP) QDs.

Materials. Anhydrous zinc acetate (Zn, <99.9%), indium(III) acetate (In, 99.99%), and trioctylphosphine (TOP, 90%) were procured from Thermo Scientific and used as received. Tris(trimethylsilyl)phosphine (TMS3P, 98%) was procured from Strem Chemicals and used as received. Palmitic Acid (PA, <99%) was procured from MP Biomedicals and used as received. 1-octadecene (ODE, 90%), anhydrous toluene (Tol, 99.8%), and acetone (<99.5%) were procured from Sigma Aldrich and used as received.

In Precursor Preparation. 0.15 mmol In powder (440 mg), 0.125 mmol Zn powder (320 mg), and 0.5 mmol PA powder (1500 mg) were combined in 100 mL ODE (100 mL) inside a round bottom flask. This mixture was heated at 130°C under vacuum for 5 h until a clear and transparent solution was formed. The obtained stock solution was then allowed to cool to room temperature under an inert environment.

P Precursor Preparation. 5 ml of TMS3P was mixed with 50 ml of TOP in a 60 mL vial inside a glove box. The solution was stirred overnight to become a colorless solution and left in the glove box until use. For each reaction, 1 ml of the prepared stock solution was diluted with 3 ml of TOP.

Synthesis Platform. The flow reactor consisted of three heated reactor sections, similar to the one used for CdSe QD synthesis, set to 113°C, 162°C and 284°C with volumes of 803µL, 534µL, and 1366µL each. The τ_0 = 4 min, ramped at α = 0.42 for a duration of 25.5 min; the volumetric flowrate ratio between both In and P precursor was maintained constant at 11.2:1. Two distinct and independent SSFEs were carried out at τ = 5 min and 7 min. The obtained DFE to SSFE mapping for high-temperature synthesis of InP nanocrystals is presented in **Supplementary Figure 6** for a target optical feature, that is the first excitonic peak absorbance divided by the first excitonic valley (P/V ratio). This successful DFE vs. SSFE mapping of an exemplary III-V QDs, demonstrate the generalizability of the developed data intensification strategy for accelerated and material-efficient synthesis space exploration of inorganic materials with high-dimensional spaces.

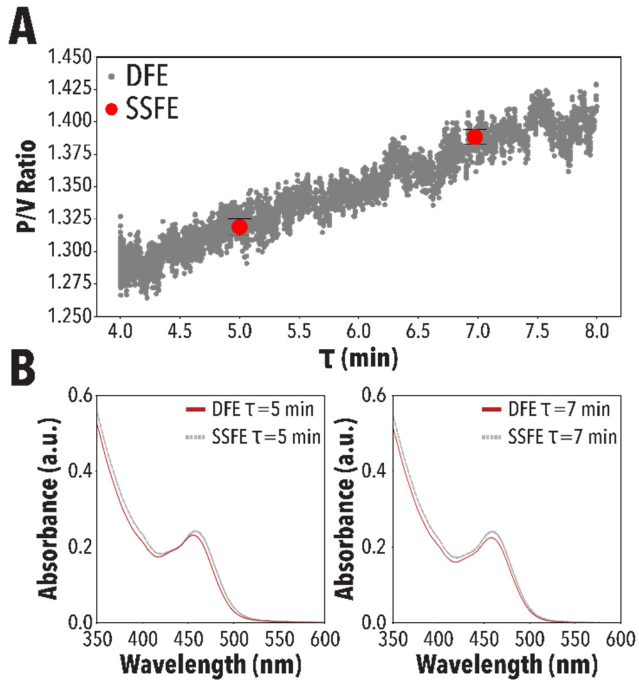

Supplementary Figure 6. DFE *vs.* SSFE for InP QDs. (A) *The peak-to-valley (P/V) ratio obtained from the first excitonic peak of the absorption spectra is calculated for DFE and compared to independent SSFE (red points) conducted at τ = 5 min and 7 min. Each point represents the mean of 15 s of the P/V ratio and error bars represent two standard deviations within the same time interval. (B) Overlay of the UV-Vis absorption spectra of the transient data extracted from the DFE with steady-state data from SSFE at identical τ.*

6. Automated and Autonomous Workflows

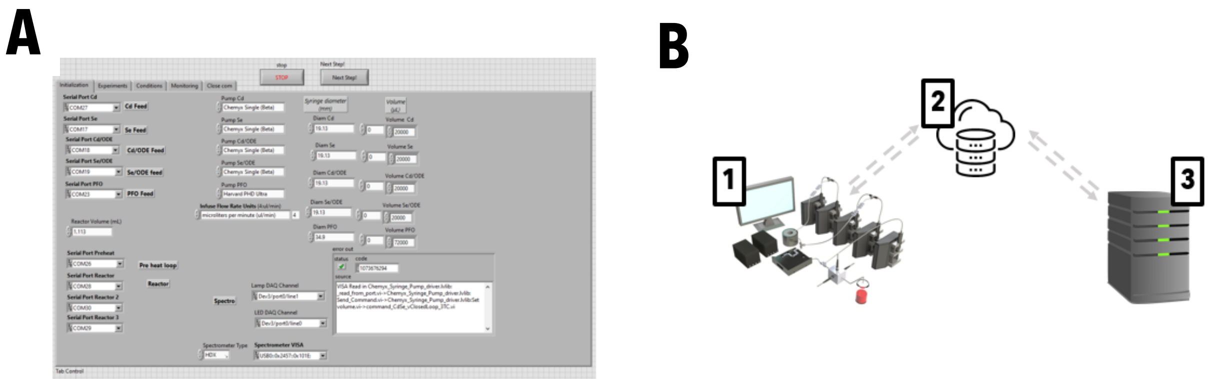

Supplementary Figure 7. Developed Workflow for Automated/Autonomous In-Flow QD Synthesis. *(A) A screenshot of the bespoke LabVIEW user interface developed for control and monitoring of the self-driving fluidic lab hardware. (B) Schematic representation of the autonomous experimentation workflow: (1) Control module, edge computing responsible for automated QD synthesis in flow, in-situ characterization, and real-time data processing; (2) Cloud database for real-time data storage, sharing, and visualization; and (3) inference module, local server computation for autonomous experimentation planning.*

LabVIEW (National Instruments version 24.0) served as the primary interface for both automated dynamic experimentation and steady-state autonomous optimization process control module. A snapshot of the custom-developed LabVIEW interface is shown in **Supplementary Figure 6**. Two distinct experimental protocols were implemented. For DFEs, the system accepts a CSV file containing key DFE process parameters: initial and final residence times, ramp duration, corresponding Cd and Se concentrations, and the preheater and microreactor temperatures. For steady-state closed-loop optimization experiments, a separate CSV file specifies individual volumetric flow rates for each precursor syringe (*Cd*, *Se*, ODE_{Cd}, and ODE_{Se}) along with the preheater and microreactor temperatures. Both protocols incorporate two configurable waiting periods: a "Residence Time Wait" (specified as a multiple of the nominal residence time) and a "Generic Wait" (specified in minutes). In a typical experimental run, the system undergoes a "Residence Time Wait" factor of 3.5 to ensure steady-state conditions (*e.g.,* a 3.5 min wait for a 1 min residence time condition), followed by a 5-min "Generic Wait" period for sample collection. Upon completion of these waiting periods (which can be manually overridden), the system flags the next 10 *in-situ* measurements as steady-state data before proceeding with the experiment (*i.e.,* either volumetric flow rate linear ramp or standby for the next suggested experiment). Between each experimental condition, both protocols execute a temperature stabilization period (ensuring ±1°C from setpoint) during which pure ODE flows through both the preheater and microreactor at 500 µL/min to wash the entire fluidic path, ensuring experiment-to-experiment independence. Data collection begins immediately after the temperature stabilization period is complete. A custom-built Python script processes the acquired raw spectra in real-time (through parallelization), extracting key optical features and uploading them to a MongoDB database (version 8.0.3) where it can be accessed and visualized by authorized users.

The steady-state autonomous optimization workflow integrates both the control module described above and the inference module that is located at an external server, as seen in **Supplementary Figure 6.** At the beginning of each experiment, the control module (**[1], Supplementary Figure 6**), creates a *document* specifying the datetime stamp of the start of the run, the experiment number, and the datetime stamp of the start of the given experiment. These *documents* reside in the cloud (**[2], Supplementary Figure 6**) in a *collection* called 'start_times'. Data that is processed in real-time resides in two distinct *collections* called 'spectra_processed' and 'parameters' where key optical features (*i.e.,* λ_{em}, *FWHM*, absorbance at excitation) and process parameters (*i.e.,* volumetric flow rates and preheater and reactor temperatures) were captured, respectively. Each *document* in these *collections* contains information about their 'experiment', 'start_run', and 'stability' flag, which is later used by the inference module (**[3], Supplementary Figure 6**) to keep track of the current experiment and suggest new experimental conditions based on previously suggested experiments and initialization data.

The BO workflow in the inference module utilizes a Single Task GP (radial basis function kernel) for each output parameter (*i.e.,* λ_{em} and *FWHM*). Process inputs and outputs were normalized according to **Supplementary Equations 4–11**. The volumetric flow rate inputs are constructed in such a way that a volumetric flow ratio of 1:5 cannot be exceeded. This threshold was chosen to preserve flow stability. The objective function is constructed as a weighted distance between a target emission wavelength and FWHM, shown in **Supplementary Equation 12.** For all experimental campaigns, the objective function weights were constant (15.4 and 1 for the $\lambda_{em}$and *FWHM*, respectively). The target for *FWHM* was maintained constant at 10 nm, while the λ_{em} was varied as desired.

$$X_1 = \frac{\dfrac{Cd}{Cd + Cd_{ODE}} - \dfrac{1}{6}}{\dfrac{5}{6} - \dfrac{1}{6}} \quad \text{(Supplementary Equation 4)}$$

$$X_2 = \frac{\dfrac{Se}{Se + Se_{ODE}} - \dfrac{1}{6}}{\dfrac{5}{6} - \dfrac{1}{6}} \quad \text{(Supplementary Equation 5)}$$

$$X_3 = \frac{\dfrac{Cd + Cd_{ODE}}{Cd + Cd_{ODE} + Se + Se_{ODE}} - \dfrac{1}{6}}{\dfrac{5}{6} - \dfrac{1}{6}} \quad \text{(Supplementary Equation 6)}$$

$$Tau = \frac{\dfrac{V_{Reactor}}{Cd + Cd_{ODE} + Se + Se_{ODE}} - 0.5}{10 - 0.5}, \; V_{Reactor} = 1113\ \mu L \quad \text{(Supplementary Equation 7)}$$

$$T_{pre} = \frac{T_{preheater} - 220}{290 - 220} \quad \text{(Supplementary Equation 8)}$$

$$T_{rxn} = \frac{T_{reactor} - 220}{290 - 220} \quad \text{(Supplementary Equation 9)}$$

$$Emmission_{Wavelength} = \frac{Peak\ Emmission_{wavelength} - 450}{670 - 450} \quad \text{(Supplementary Equation 10)}$$

$$FWHM = \frac{FWHM - 110}{10 - 110} \quad \text{(Supplementary Equation 11)}$$

$$\min_{i \in \{Emission\ Wavelength,\ FWHM\}} - \left|\left| w_i \cdot \left(\overline{Y}_{sample_i} - Y_{target_i} \right) \right|\right|_2^2$$ (Supplementary Equation 12)

Each BO campaign conducted with the SDFL had an experimental budget of 10 steady-state experiments. Expected improvement (EI) was used as the decision-making policy during the BO campaign; however, for experiments 5 and 10 (*i.e.,* halfway through the BO campaign and the last experiment) the decision-making policy was changed to pure exploitation (*i.e.,* upper confidence bound with $\beta = 0$). The new BO-predicted experimental condition is sent by the inference module (**[3], Supplementary Figure 6**) to a *collection* called 'new_conditions' at the database (**[2], Figure S6C**), that the control module (**[1], Supplementary Figure 6**) monitors during standby, and then writes to the CSV file, thus closing the loop.

7. Closed-Loop Optimization Data

Supplementary Table 5. *Summary of the autonomous CdSe QD synthesis data.*

Target (nm)	Iteration #	Tau (min)	Tpre (°C)	Trxn (°C)	Cd (µL/min)	Se (µL/min)	CdODE (µL/min)	SeODE (µL/min)	λem (nm)	FWHM (nm)
540	1	0.62	262.51	265.68	132.04	768.57	297.88	603.97	544.29	41.16
	2	0.61	261.49	265.62	63.66	847.07	238.22	662.35	550.59	34.73
	3	0.82	234.34	279.89	296.56	161.26	648.20	245.33	545.06	31.36
	4	0.62	238.22	278.45	379.59	217.50	881.61	318.61	539.17	32.16
	5	0.64	233.99	279.12	387.38	209.20	825.79	307.49	538.89	31.37
	6	0.50	231.11	278.05	414.78	294.65	1135.57	381.00	539.35	31.21
	7	0.68	231.54	276.47	294.76	224.75	765.12	358.43	539.53	35.17
	8	0.63	229.63	280.22	487.81	196.94	890.46	199.02	540.33	30.54
	9	0.90	271.96	277.06	196.86	202.87	654.71	186.29	545.99	30.32
	10	0.60	271.23	277.03	297.48	295.29	990.37	275.04	547.35	30.73
560	1	2.43	259.49	277.59	63.77	92.96	205.64	95.83	558.42	41.55
	2	1.97	263.42	269.45	50.18	262.24	90.45	161.61	558.72	40.25
	3	2.72	264.40	264.85	14.77	166.59	64.67	162.51	556.18	32.50
	4	2.53	256.50	264.12	15.49	204.05	65.28	155.22	557.66	32.55
	5	2.77	261.56	264.25	15.42	177.06	58.91	149.75	559.40	34.43
	6	2.79	253.44	264.68	17.15	157.85	60.91	162.35	558.19	35.60
	7	2.95	280.28	276.14	34.39	81.71	171.94	89.78	559.25	39.08
	8	2.48	262.26	270.59	15.19	222.53	75.95	135.31	561.42	31.86
	9	2.10	251.80	268.66	16.38	287.29	81.91	144.86	556.57	29.03
	10	2.45	255.29	268.43	14.96	233.01	71.31	135.47	559.19	31.10

580	1	8.04	264.56	277.88	19.92	27.29	62.10	29.17	576.37	35.54
	2	8.11	263.13	267.84	11.33	63.91	19.82	42.21	576.79	35.34
	3	8.44	272.36	278.11	15.69	18.60	66.10	31.44	575.49	35.35
	4	8.08	265.52	276.35	22.90	65.28	23.06	26.59	580.65	35.86
	5	3.61	251.60	287.19	47.60	177.87	28.40	54.51	579.53	35.76
	6	8.71	278.58	273.82	17.90	34.41	50.75	24.73	577.07	35.50
	7	7.24	281.65	265.88	28.89	70.17	20.41	34.20	577.51	40.00
	8	8.28	253.42	267.21	7.92	63.32	20.17	42.95	576.90	34.36
	9	7.66	241.77	279.18	28.31	21.88	67.26	27.92	579.14	37.89
	10	8.01	278.47	273.81	28.13	55.28	30.75	24.75	579.20	37.40
600	1	9.20	253.04	252.80	54.58	13.99	25.64	26.83	596.54	53.49
	2	10.00	248.21	259.96	53.72	6.90	24.09	26.59	609.77	49.70
	3	9.74	258.98	250.52	61.18	13.96	17.07	22.08	598.45	47.15
	4	10.00	250.39	249.30	68.33	9.69	18.20	15.08	600.83	46.23
	5	10.00	257.13	251.64	61.09	12.19	16.94	21.08	600.80	46.38
	6	10.00	270.92	258.18	54.98	13.69	21.14	21.49	601.50	50.55
	7	10.00	256.29	260.65	55.33	18.94	11.68	25.35	597.05	47.71
	8	10.00	245.53	244.17	71.08	7.39	14.22	18.61	594.72	50.76
	9	9.27	239.26	277.69	46.42	7.21	50.06	16.44	611.70	53.77
	10	10.00	249.53	248.02	71.88	5.96	14.37	19.09	599.20	50.17

8. Particle Size Distribution from TEM Images

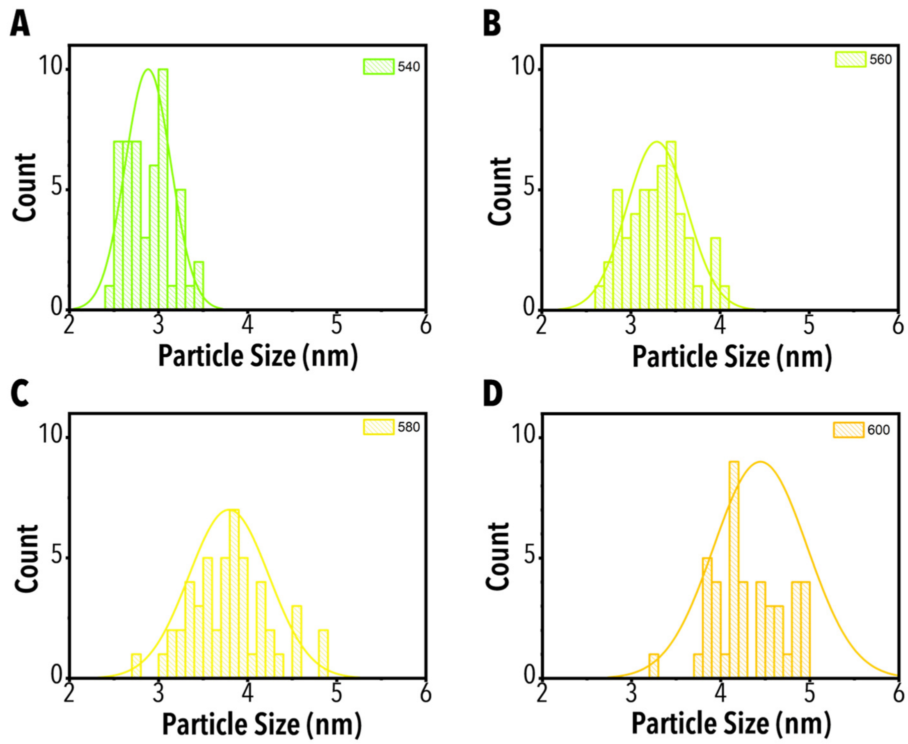

Supplementary Figure 8. CdSe QD Size Distribution. *Size distribution histograms of autonomously manufactured CdSe nanocrystals (50 counts) by the SDFL at* λ_{em} *values of (A) 540 nm, (B) 560 nm, (C) 580 nm, and (D) 600 nm*.

9. Continuous Nanomanufacturing of the Targeted Wavelength

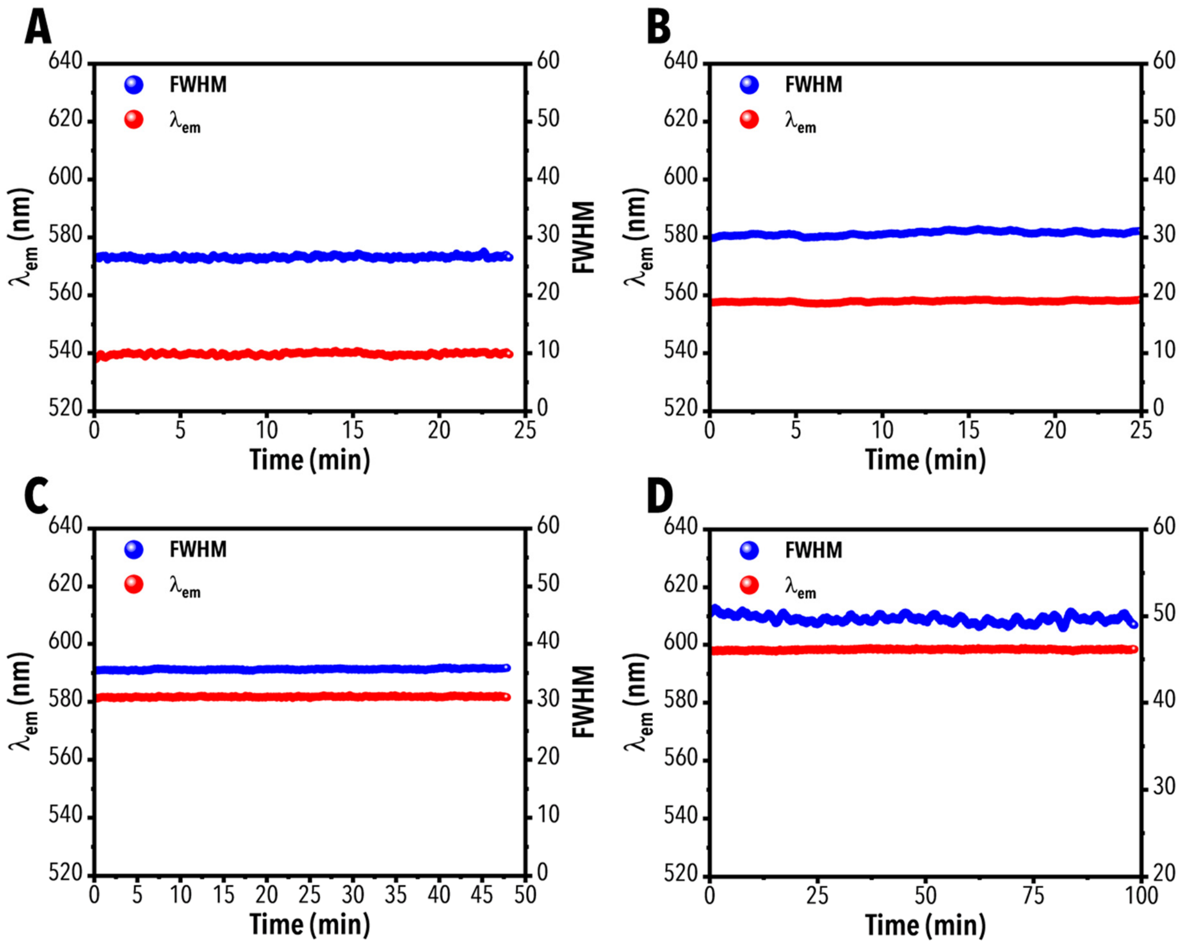

Supplementary Figure 9. Continuous Nanomanufacturing of CdSe QD. *Continuous nanomanufacturing of 20 mL of CdSe QDs using the synthetic routes discovered by the SDFL at* λ_{em} *values of (A) 540 nm, (B) 560 nm, (C) 580 nm, and (D) 600 nm.*

Supplementary References

1 Levenspiel, O. *Chemical reaction engineering*. (John wiley & sons, 1998).

2 Saxena, A. & Nigam, K. Coiled configuration for flow inversion and its effect on residence time distribution. *AIChE Journal* **30**, 363-368 (1984).

3 López-Guajardo, E., Ortiz-Nadal, E., Montesinos-Castellanos, A. & Nigam, K. D. Coiled flow inverter as a novel alternative for the intensification of a liquid-liquid reaction. *Chemical Engineering Science* **169**, 179-185 (2017).

4 Mridha, M. & Nigam, K. Coiled flow inverter as an inline mixer. *Chemical engineering science* **63**, 1724-1732 (2008).

5 Klutz, S., Kurt, S. K., Lobedann, M. & Kockmann, N. Narrow residence time distribution in tubular reactor concept for Reynolds number range of 10–100. *Chemical Engineering Research and Design* **95**, 22-33 (2015).

6 Moore, J. S. & Jensen, K. F. "Batch" kinetics in flow: online IR analysis and continuous control. *Angewandte Chemie International Edition* **53**, 470-473 (2014).

7 Florit, F. *et al.* Dynamic flow experiments for Bayesian optimization of a single process objective. *Reaction Chemistry & Engineering* **10**, 656-666 (2025).

8 Liu, H., Cai, J., Ong, Y.-S. & Wang, Y. Understanding and comparing scalable Gaussian process regression for big data. *Knowledge-Based Systems* **164**, 324-335 (2019).